Adenosine A2a Receptor Antagonism Restores Additive Cytotoxicity by Cytotoxic T Cells in Metabolically Perturbed Tumors

Jeroen Slaats[1], Esther Wagena[1], Daan Smits[1], Annemarie A. Berends[1], Ella Peters[1], Gert-Jan Bakker[1], Merijn van Erp[1], Bettina Weigelin[1,2,3], Gosse J. Adema[4], and Peter Friedl[1,5]

ABSTRACT

Cytotoxic T lymphocytes (CTL) are antigen-specific effector cells with the ability to eradicate cancer cells in a contact-dependent manner. Metabolic perturbation compromises the CTL effector response in tumor subregions, resulting in failed cancer cell elimination despite the infiltration of tumor-specific CTLs. Restoring the functionality of these tumor-infiltrating CTLs is key to improve immunotherapy. Extracellular adenosine is an immunosuppressive metabolite produced within the tumor microenvironment. Here, by applying single-cell reporter strategies in 3D collagen cocultures *in vitro* and progressing tumors *in vivo*, we show that adenosine weakens one-to-one pairing of activated effector CTLs with target cells, thereby dampening serial cytotoxic hit delivery and cumulative death induction. Adenosine also severely compromised CTL effector restimulation and expansion. Antagonization of adenosine A2a receptor (ADORA2a) signaling stabilized and prolonged CTL–target cell conjugation and accelerated lethal hit delivery by both individual contacts and CTL swarms. Because adenosine signaling is a near-constitutive confounding parameter in metabolically perturbed tumors, ADORA2a targeting represents an orthogonal adjuvant strategy to enhance immunotherapy efficacy.

Introduction

Cytotoxic T lymphocytes (CTL) are antigen-specific effector cells with the ability to eradicate cancer cells in a contact-dependent manner. The presence of CTLs in solid tumors positively correlates with improved clinical outcomes across a broad range of tumor types (1). Consequently, strategies have been developed to augment T-cell infiltration into the tumor microenvironment, including adoptive T-cell transfer (ACT) and dendritic cell (DC) vaccination (2, 3). However, although these strategies favor accumulation of tumor-specific CTLs in the tumor, only a fraction of patients reach tumor rejection and long-term survival (4–6). The mechanisms underlying this clinical failure are diverse, including CTL paralysis induced by an immunosuppressive tumor microenvironment (7). Thus, overcoming immunosuppression in tumors represents an unmet need for improving CTL effector function and anticancer immunotherapy.

The efficacy of the CTL effector response critically depends on the multistep recognition and elimination of antigenic target cells. Activated CTLs in the tumor probe the local tissue microenvironment in search for antigenic target cells. Target cell recognition initiates a stop signal to slow down CTL migration, thereby facilitating prolonged CTL engagement and the formation of an immune synapse (8). The immune synapse mediates cell–cell interaction and T-cell signaling to trigger the release of perforins and granzymes toward the target cell (9). Cytotoxic contacts are terminated upon CTL detachment from the target cell, followed by interstitial CTL migration and subsequent engagements with neighboring target cells (10, 11). The cytototoxic attack of CTL against solid tumor cells is inefficient and rarely completed by a single CTL. Instead, multiple CTLs sequentially engage with the same target cell to deliver a sequence of sublethal hits that accumulate overtime to induce target cell death (termed additive cytotoxicity; ref. 12). This complex sequence of migration, adhesion, and signaling steps enables serial killing and CTL cooperation to eliminate tumor cells.

Immunosuppressive factors released in tumor lesions have been shown to interfere with the CTL effector response. The nucleoside adenosine constitutes a potent immunosuppressive metabolite in the tumor microenvironment. While present at nanomolar concentrations in healthy tissues, extracellular adenosine accumulates up to micromolar levels in solid tumors, with higher concentrations in the tumor core than in the periphery (13, 14). The majority of adenosine in the tumor interstitium comes from the sequential hydrolysis of extracellular ATP by the cell-surface enzymes CD39 and CD73. In preclinical animal models, targeted inhibition of these ectonucleotidases restores antitumor immunity and enhances the efficacy of cancer immunotherapies (15–19). In addition, CD39 and CD73 predict poor clinical outcomes in various human cancers (20). Extracellular adenosine exerts its biological functions through activation of G-protein–coupled adenosine receptors (A1, A2a, A2b, and A3), which are differentially expressed on tumor, stromal, and infiltrating immune cells. The adenosine A2a receptor (ADORA2a) is the predominant subtype expressed by CTLs (21). ADORA2a signaling reduces T-cell crawling on ICAM-1 substrates that mimic cell surfaces (22). Adenosine also activates the C-terminal Src kinase (Csk) in naïve CTLs, which exerts tonic inhibition of the Src family kinases Lck

[1]Department of Cell Biology, Radboud Institute for Molecular Life Sciences (RIMLS), Radboud University Medical Center, Nijmegen, the Netherlands. [2]Department of Preclinical Imaging and Radiopharmacy, Eberhard Karls University Tübingen, Tübingen, Germany. [3]Cluster of Excellence iFIT (EXC 2180) "Image-Guided and Functionally Instructed Tumor Therapies," University of Tübingen, Tübingen, Germany. [4]Radiotherapy and Onco-Immunology Laboratory, Department of Radiation Oncology, Radboud University Medical Center, Nijmegen, the Netherlands. [5]Department of Genitourinary Medicine, University of Texas MD Anderson Cancer Center, Houston, Texas.

Corresponding Author: Peter Friedl, Cell Biology, Radboud University Nijmegen Medical Centre, Post 283, PO Box 9101, Nijmegen 6500HB, the Netherlands. E-mail: peter.friedl@radboudumc.nl

Cancer Immunol Res 2022;10:1462–74

doi: 10.1158/2326-6066.CIR-22-0113

and Fyn, thereby dampening the strength of T-cell receptor (TCR) signaling (23, 24). The bulk suppressive effect of adenosine/ADORA2a signaling on CTL-mediated antitumor immune control has been well established (14, 25, 26), yet the impact on the individual substeps and associated contact kinetics of the CTL effector response remain obscure.

Understanding the cellular and molecular mechanisms by which adenosine compromises CTL effector function requires time-resolved analysis of the multistep CTL effector response at cellular and molecular levels. We used single-cell reporter strategies to detect perforin hit delivery toward antigenic B16F10 melanoma cells in 3D collagen coculture *in vitro* and progressing tumors *in vivo*. This revealed that adenosine destabilizes CTL–target cell contacts, which resulted in reduced perforin hit delivery and target cell killing. Pharmacologic inhibition of ADORA2a restored target cell killing by stabilizing CTL–tumor cell interactions and increasing repetitive hit delivery. This identifies the adenosine–ADORA2a signaling axis in perturbing sublethal multihit delivery, which can be restored by ADORA2a antagonism.

Materials and Methods

Cells and cell culture

Mouse melanoma B16F10 cells were obtained from ATCC (CRL-6475). B16F10 cells expressing the ovalbumin-derived CTL epitope SIINFEKL were obtained by electroporation. Stable H2B-GFP- or H2B-mCherry–expressing B16F10/OVA cells were obtained by lentiviral transduction and blasticidin selection (10 mg/mL; Thermo Fisher Scientific, R2101). B16F10/OVA H2B-mCherry cells were lentivirally transduced to stably express the calcium sensor GCaMP6s followed by blasticidin selection (10 mg/mL; ref. 27). The cells were cultured in RPMI-1640 medium (Gibco, 21875-034) supplemented with 10% FCS (Sigma, F7524), 1% sodium pyruvate (Gibco, 13360-039), and 1% penicillin and streptomycin (PAA, P11-010). OT-I CTLs (discussed below) were cultured in T-cell medium (TCM), consisting of RPMI-1640 (Gibco, 21875-034) supplemented with 10% FCS (Sigma, F7524), 10 mmol/L HEPES (Gibco, 15630-056), 500 mmol/L 2-mercaptopethanol, 1% penicillin, and streptomycin (PAA, P11-010), 1% sodium pyruvate (GIBCO, 11360-039), and 0.1 mmol/L nonessential amino acids (Gibco, 11140-035). During 3D collagen interface coculture, CTLs were cultured in TCM containing heat-inactivated FCS (15 minutes at 80°C) to limit FCS-induced metabolic breakdown of adenosine. Cell culture was performed at 37°C in a humidified 5% CO_2 atmosphere. Identity of the B16F10 cells was verified by short tandem repeat (STR) DNA profiling (IDEXX BioResearch, last profiled in May 2018). No mammalian interspecies contamination was detected. Lack of contamination with *Mycoplasma* was routinely verified using the MycoAlert Mycoplasma Detection Kit (Lonza, LT07-318, last tested in August 2020). Cell lines were cultured up to a maximum of 30 passages.

Isolation and activation of primary murine $CD8^+$ OT-I T lymphocytes

Splenocytes were derived from spleens of OT-I TCR transgenic mice (Jackson Laboratories, stock number: 003831) or from double-transgenic dsRed/OT-I mice obtained by crossing dsRed. T3 mice (Jackson Laboratories, stock number: 006051) with OT-I TCR transgenic mice (Jackson Laboratories, stock number: 003831). Splenocytes and OT-I T lymphocytes were cultured in TCM (see above). Splenocytes were harvested by mashing the spleen tissue through a 100-μm nylon cell strainer (BD, 352360). Erythrocytes were depleted by incubating the splenocytes in ammonium chloride (0.83% NH_4Cl, 0.1% $KHCO_3$, 0.37% Na_2EDTA; 5 minutes at room temperature).

For the expansion of antigen-specific CTLs, splenocytes were cultured in TCM in 24-well plates (5×10^5 cells/well) in the presence of SIINFEKL peptide (0.5 μg/mL; Sigma-Aldrich, S7951). After 3 days of culture, the cells were resuspended in a mixture of 50% CTL expansion culture supernatant with 50% fresh TCM and cultured in 24-well plates (4×10^5 cells/well) in the presence of IL2 (100 units/mL; ABD Serotec, PMP38). After 48 hours of culture, CTLs were isolated by Ficoll gradient centrifugation (Axis-Shield, 1114544). Purity typically exceeded 96% $V\alpha2^+CD8^+CD62L^{low}CD44^{hi}$ cells, as determined by flow cytometry (BD FACSCalibur or BD FACS Lyric) using PerCP-Cy5.5–conjugated rat antimouse CD8a (BD Biosciences, 551162), APC-conjugated rat antimouse Va2 TCR (BD Biosciences, 560622), FITC-conjugated rat antimouse CD62 L (BD Biosciences, 561917), and PE-conjugated rat antimouse CD44 (BD Biosciences, 553134).

3D interface coculture

Unless stated otherwise, B16F10/OVA target cells were stimulated with interferon-gamma (IFNγ, 200 units/mL; PeproTech, 315-05) for 24 hours prior to seeding to enhance SIINFEKL antigen presentation (28). Target cells were seeded in a 96-well flat bottom plate (7,000 B16F10/OVA cells/well with 200 units/mL IFNγ) and allowed to adhere and spread overnight to form a subconfluent target cell layer. Preactivated OT-I CTLs were resuspended in bovine collagen solution (1.7 mg/mL; Advanced BioMatrix, 5005) and overlaid onto the target cell monolayer at CTL-target cell ratios ranging from 4:1 to 1:16. After collagen polymerization (30 minutes at 37°C), TCM was added to each well and the coculture was incubated for 30 hours. For proliferation analysis, preactivated OT-I CTLs were stained with 400 nmol/L CFSE (10 minutes at room temperature; Thermo Fisher, C1157) prior to embedding in the collagen matrix. The 3D cytotoxicity cocultures were treated with adenosine (25 μmol/L or 50 μmol/L; Sigma-Aldrich, A4036) and ADORA2a antagonist ZM-241385 (0.5 μmol/L; Tocris, 1036). CTL proliferation, viability, and cell-surface CD107a expression were assessed via flow cytometry as described below.

Analysis of viable cells by flow cytometry

Cells were harvested from the 3D interface coculture by enzymatic digestion of the collagen gel using collagenase I (190 U/well, 30 minutes at 37°C; Sigma-Aldrich, C0130). The resulting cell suspension was collected, and the remaining adherent cells were detached using trypsin (0.075%; Gibco, 15090046) and EDTA (1 mmol/L; Invitrogen, 15575020). The cell suspension after trypsin/EDTA treatment was combined with the cell suspension after collagen digestion (without centrifugation), and the whole volume was analyzed by flow cytometry using a BD FACSCalibur and BD FACS Lyric. For measuring the effect of adenosine on CTL viability, OT-I CTLs (1.05×10^5 cells) were maintained in 2D culture in TCM for 6 hours without target cells in the absence (milliQ) or presence of adenosine (50 μmol/L) and analyzed by flow cytometry. To determine cell-surface expression of CD107a, cells were stained with Alexa Fluor 488–conjugated anti-mouse CD107a (20 μg/mL; BioLegend, 121608) or the respective isotype control (20 μg/mL; BioLegend, 400525) in ice-cold PBS for 1 hour. After incubation, cells were stained with Alexa Fluor 488-conjugated donkey anti-rat antibody (5 μg/mL; Thermo Fisher, A-21208) in ice-cold PBS for 1 hour. Cells were gated on intact morphology, viability by propidium iodide (Sigma-Aldrich, P4170) or Sytox Blue (Thermo Fisher Scientific, S11348) exclusion, and dsRed expression using FlowJo

software (Tree Star, version 10; Supplementary Fig. S1a). For CTL proliferation analysis, the CFSE signal intensity was determined after gating for viable dsRed-labeled CTLs.

Brightfield time-lapse microscopy

B16F10/OVA target cells were stimulated with IFNγ (200 units/mL; PeproTech, 315-05) for 24 hours prior to seeding to enhance SIINFEKL antigen presentation (28). Target cells were seeded in a 96-well flat bottom microplate (7000 B16F10/OVA cells/well with 200 units/mL IFNγ; Greiner Bio-One, 665090) and allowed to adhere and spread overnight to form a subconfluent target cell layer. Preactivated OT-I CTLs were resuspended in bovine collagen solution (1.7 mg/mL; Advanced BioMatrix, 5005) and overlaid onto the target cell monolayer at a CTL–target cell ratio of 1:1. After collagen polymerization (30 minutes at 37°C), TCM was added, and the coculture was monitored by brightfield time-lapse microscopy using a BD Pathway 855 High-Content Bioimager with a plan -NEOFLUAR 10x/0.3 air objective and Modicam Olympus UApo/340 20×/0.75 or Zeiss Axiovert 200M with Moticam-pro 2850 CCD Camera in an OKOlab stage-top CO_2 incubator. Images were taken with a 30- to 98-second frame interval for up to 30 hours.

The duration, kinetics, and killing outcome of individual CTL–target cell interactions were quantified by manual analysis. CTLs migrating in an out-of-focus plane above the target cell in the 3D collagen matrix were not included for analysis. Direct CTL–target cell contacts were identified based on the following morphologic and kinetic criteria: polarization/flattening of the CTL on the target cell-surface, deviation of the CTL migration path along the target cell-surface, and slowed CTL migration speed or migration arrest. For analyzing the effect of adenosine on CTL migration speed, CTL migration in 3D interface cocultures was quantified during periods without conjugation to B16F10/OVA cells using computer-assisted cell tracking (AutoZell 1.0 Software; Center for Computing and Communication Technologies, University of Bremen, Bremen, Germany).

Monitoring calcium flux in OT-I CTLs during target cell conjugation

Preactivated OT-I CTLs (3.6×10^6 cells/mL) were incubated with Fura-2 AM (2 μmol/L, 30 minutes, 37°C, in the dark; Thermo Fisher, F1221), washed twice with TCM and embedded in the 3D interface coculture with unlabeled B16F10/OVA target cells as described above. Ca^{2+} signals in the OT-I CTLs were monitored by spinning-disk confocal microscopy (BD Pathway 855 High-Content Bioimager; Olympus UApo/340 20×/0.75) using a frame interval of 104 to 112 seconds. To account for phototoxicity and bleaching, imaging periods were limited to 1 hour. CTL calcium fluxes were analyzed by manual region-of-interest (ROI) selection using the Fura-2 340/380 ratiometric images.

Monitoring calcium events in target cells

B16F10/OVA target cells were engineered to stably express the calcium sensor GCaMP6s (27). 3D cocultures of target cells and CTLs were set up as described above. CTL–target cell conjugation and associated intracellular Ca^{2+} events were obtained by long-term confocal microscopy of GCaMP6s and OT-I CTLs at frame intervals of 8 to 15 seconds for up to 12 hours (Leica SP8 SMD; Leica HC PL APO CS 40×/0.85) using a fixed focus, 600 μm optical section, and an excitation power of 0.05 mW for each 488 and 561 nm laser line (3.16 μsec pixel dwell time, 0.32 μm^2 pixel size). Lack of phototoxicity was verified based on unperturbed migration (CTL) and morphologic integrity (CTL, target cells). OT-I CTL interaction kinetics were coregistered with Ca^{2+} events and B16F10/OVA death induction. Target cell death was identified by increased GCaMP6s sensor brightness, followed by cell shrinkage. CTL-associated Ca^{2+} events were identified by manual frame-by-frame image intensity analysis and displayed for cell populations of multiple independent experiments.

Quantitative reverse transcription PCR

B16F10/OVA target cells were stimulated with IFNγ (200 units/mL; PeproTech, 315-05) for 24 hours. B16F10/OVA target cells (5×10^5 cells) or preactivated OT-I T cells (2×10^6) were lysed using Buffer RLT (Qiagen, 79216) containing 1% β-mercaptoethanol. After mechanical homogenization of the lysate using a cell scraper, RNA was isolated using the RNeasy Micro Kit (Qiagen, 74004), and total RNA was reverse transcribed using the iScript cDNA Synthesis Kit (Bio-Rad, 1708890). Primers were designed using HomoloGene (**Table 1**; http://www.ncbi.nlm.nih.gov). Primers were validated *in silico* using Oligoanalyzer software (http://www.idtdna.com/analyzer/Applications/OligoAnalyzer/). Quantitative PCR was performed on a CFX96 Real-Time PCR Detection System with C1000 Thermocycler (Bio-Rad) and analyzed using the Bio-Rad CFX Maestro software (version 4.1.2433.1219). RNA expression for the genes of interest was normalized to the pooled levels of two housekeeping genes (*Gapdh* and *Hprt1*).

Analysis of phospho-src^+ microclusters in preactivated CTLs

A 96-well flat-bottom microplate (Greiner Bio-One, 665090) was coated overnight with anti-mouse CD3ε (10 μg/mL; BioLegend, 100339). Preactivated CTLs (3×10^6 cells/mL) were incubated in the absence (DMSO) or presence of ZM-241385 (0.5 μmol/L, 15 minutes at 37°C; Tocris, 1036), followed by the addition of milliQ water or adenosine (50 μmol/L, 30 minutes at 37°C; Sigma-Aldrich, A4036). The CTL suspension was added to the anti-CD3–coated microplate (150,000 CTLs/well) and incubated (10 minutes at 37°C), followed by fixation with Bouin solution (15 minutes, room temperature; Klinipath, 64096). After permeabilization (15 minutes, room temperature); 1× PBS, 0.1% Triton X-100 (Sigma-Aldrich, T8787), 10% normal goat serum (Thermo Fisher Scientific, PCN5000), 1% BSA

Table 1. Forward and reverse primers used for quantitative PCR.

	Forward sequence	Reverse sequence
A1	ACC TCC GAG TCA AGA TCC CTC	CTC ACT CAG GTT GTT CCA GCC
A2a	CCA GAG CAA GAG GCA GGT ATC	TGA CTT CTA CAG GGG GTC CG
A2b	CGT CCC GCT CAG GTA TAA AGG T	CAA AGG CAA GGA CCC AGA GG
A3	TTG CCT TCA GGT GCT CAG CTA	CCG TTC TAT ATC TGG ATT CTC AGC G
Gapdh	GTC GGT GTG AAC GGA TTT G	GAA CAT GTA GAC CAT GTA GTT G
Hprt1	CCT AAG ATG AGC GCA AGT TGA A	CCA CAG GAC TAG AAC ACC TGC TAA

(Sigma-Aldrich, A9647), and blocking of nonspecific binding sites (1 hour, room temperature); 1× PBS, 0.05 Tween-20 (Sigma-Aldrich, P7949), 10% normal goat serum, 1% BSA), the cells were stained with anti–phospho-Src (Tyr-416) family kinase (2.5 μg/mL; Cell Signaling Technology, 2101) and Alexa Fluor 647–conjugated anti-CD45 (2.5 μg/mL; BioLegend, 103124) overnight at 4°C in blocking solution. Background staining was detected using rabbit IgG isotype control (R&D Systems, AB-105-C). Primary antibodies were detected by incubating the cells with Alexa Fluor 568–conjugated goat anti-rabbit antibody (2.5 μg/mL; Thermo Fisher, A11036) overnight at 4°C in a blocking solution. Cells were imaged using a Zeiss LSM880 (63×1.4 NA oil immersion objective, Carl Zeiss). For phospho-Src analysis, confocal microscopy was performed with sequential 561 nm and 633 nm excitation. Emission light was collected using 568 to 642 nm and 646 to 756 nm filters for Alexa Fluor 568 and Alexa Fluor 647, respectively. All images were processed using Fiji/ImageJ, and the number of phosho-Src$^+$ microclusters per CTL was analyzed using the Find Maxima plugin.

NFAT1 and granule polarization analysis in preactivated CTLs

Target cells were seeded in the presence of IFNγ (200 units/mL) in a 96-well flat bottom microplate (7,000 and 10,000 B16F10/OVA cells/well for granule polarization and NFAT1 analysis, respectively; Greiner Bio-One, 665090) and allowed to adhere and spread overnight to form a subconfluent target cell layer. Preactivated OT-1 CTLs (1.6×10^6 cells/mL) were incubated in the absence (DMSO) or presence of ZM-241385 (0.5 μmol/L, 15 minutes at 37°C; Tocris, 1036), followed by the addition of milliQ water or adenosine (50 μmol/L, 30 minutes at 37°C; Sigma-Aldrich, A4036). For granule polarization analysis, CTLs were seeded onto the subconfluent target cell layer (35,000 CTLs/well) in the presence of DMSO/ZM-241385 (0.5 μmol/L) and milliQ/adenosine (50 μmol/L) and incubated for 4 hours, followed by fixation with Bouin solution (15 minutes, room temperature; Klinipath, 64096). For NFAT1 analysis, CTLs were seeded onto the subconfluent target cell layer (80,000 CTLs/well) in the presence of DMSO/ZM-241385 (0.5 μmol/L) and milliQ/adenosine (50 μmol/L) and incubated for 4 hours, followed by fixation with 2% paraformaldehyde (PFA; 15 minutes, room temperature; Merck, 104005). After permeabilization (15 minutes, room temperature; 1× PBS, 0.1% Triton X-100, 10% normal goat serum, 1% BSA) and blocking of nonspecific binding sites (1 hour, room temperature; 1× PBS, 0.05 Tween-20, 10% normal goat serum, 1% BSA), the cells were stained with anti–phospho-Src (Tyr-416) family kinase (2.5 μg/mL; Cell Signaling Technology, 2101), anti-NFAT1 (2 μg/mL; Cell Signaling Technology, 5861), Alexa Fluor 647–conjugated anti-CD45 (5 μg/mL; BioLegend, 103124), Alexa Fluor 488–conjugated anti-granzyme B (2.5 μg/mL; Thermo Fisher, 11-8898-82) or Alexa Fluor 568 Phalloidin (200 U/mL; Thermo Fisher, A12380) overnight in blocking solution at 4°C. Background staining was detected using rabbit IgG isotype control (R&D Systems, AB-105-C). Primary antibodies were detected by incubating the cells with Alexa Fluor 647–conjugated goat anti-rabbit antibody (2.5 μg/mL; Thermo Fisher, A21245), Alexa Fluor 568–conjugated goat anti-rabbit antibody (2.5 μg/mL; Thermo Fisher, A11036) and Alexa Fluor 488–conjugated goat anti-rat antibody (2.5 μg/mL; Thermo Fisher, A11006) overnight at 4°C in blocking solution. Nuclei were stained with DAPI (1 μg/mL, 15 minutes at room temperature; Sigma-Aldrich, D9542). Imaging was performed using laser scanning microscopy (LSM880; 63 × 1.4 NA oil immersion objective; Carl Zeiss). For CTL granule polarization analysis, confocal microscopy was performed with 488 nm and 647 nm excitation, followed by 561 nm excitation. Emission light was collected using 499 to 575 nm, 578 to 644 nm, and 645 to 701 nm filters for Alexa Fluor 488, Alexa Fluor 568, and Alexa Fluor 647, respectively. For NFAT1 analysis, Airyscan imaging was performed with sequential 405, 488, 561, and 633 nm excitation. Emission light was collected using the following emission filters: BP420–480/BP495–620 for DAPI, 3P 495–550/LP 570 for Alexa Fluor 488, 3P 570–620/LP645 for Alexa Fluor 568, and 3P 570–620/LP645 for Alexa Fluor 647. Raw images were reconstructed using the Zeiss Zen 2.1 Sp1, and images were processed using Fiji/ImageJ.

Mouse model and intravital multiphoton microscopy

All experiments with mice were approved by the Ethical Committee on Animal Experiments and were performed in the Central Animal Laboratory of the Radboud University, Nijmegen (AVD10300 2019 7964), in accordance with the Dutch Animal Experimentation Act and the European FELASA protocol (https://felasa.eu/). Tumor size was continuously monitored by fluorescence microscopy, with a humane endpoint for tumors exceeding 2 cm^3.

Histone-2B/mCherry expressing B16F10/OVA cells (5×10^4 to 2×10^5) were injected into the deep dermis of C57/B16J mice (Charles River Laboratories, strain code 632) carrying a dorsal skin-fold chamber, as described (29). Three and six days after tumor implantation, *in vitro*–activated dsRed OT-I CTLs (2×10^6) were administered retro-orbitally. Tumor-bearing mice were daily monitored for up to 13 days. Intravital multiphoton microscopy was performed on anesthetized mice (1%–3% isoflurane in oxygen; Pharmachemie, 45112106). During imaging, mice were maintained on a temperature-controlled stage. Tumor volume was obtained at consecutive time points from epifluorescence overview images and calculated as $(\text{tumor width})^2 \times (\text{tumor length}) \times \pi/6$.

Intravital microscopy was performed on a customized near-infrared/infrared multiphoton microscope (TriMScope-II, LaVision BioTec a Milteny Company), equipped with two tunable Titanium: Sapphire lasers (Chameleon Ultra I and Ultra II; Coherent) and an optical parametric oscillator (MPX, APE) for excitation. Microscopy was performed using a 25 × 1.05 NA water-immersion objective lens (XLPLN25XWMP2, Olympus). Emission was filtered with 525/50 (GCaMP6s), 572/28 (dsRed), 620/60 (mCherry) and detected by alkali, GaAsP, or GaAs PMT detectors (H6780-20, H7422A-40 or H7422A-50, Hamamatsu). Time-lapse recordings of OT-I CTL effector dynamics in B16F10/OVA tumor tissue were acquired by scanning 3D tissue regions (360 μm × 360 μm × 100 μm, z-interval: 5 μm) with 1,090 nm at a laser power of 20 to 50 mW (time interval: 2 minutes, total imaging period: 60 minutes). CTL densities and B16F10/OVA mitosis/apoptosis frequencies were analyzed using 3D stacks (597 μm × 597 μm, imaging depth up to 273 μm, z-interval: 7 μm) with 1,090 nm at a laser power of 20 to 60 mW. For *in vivo* visualization of the calcium sensor GCaMP6s in B16F10/OVA cells, whole-tumor 3D stacks with an imaging depth of 308 μm (z-interval: 7 μm) were recorded with 910 nm (GCaMP6s) and 1,210 nm (mCherry) at a laser power of 15 to 35 mW. The setup was equipped with a warm plate (DC60 and THO 60-16, Linkam Scientific Instruments Ltd) and a custom-made objective heater (37°C), as described (30).

Processing and quantification of intravital images

Images were processed using Fiji/ImageJ (version 2.0.0-rc-69/1.53f, 2.0.0-rc-43/1.53i and 2.0.0-rc-43/1.52h). Images were stitched to mosaics using the Stitch Grid/Collection plugin (31), and field drifts during time-lapse recording were corrected using the StackReg plugin (32) and the Correct 3D Drift plugin (33). For image quantifications, raw, unmodified images were used. For display purposes, images were scaled and adjusted for brightness and contrast to enhance

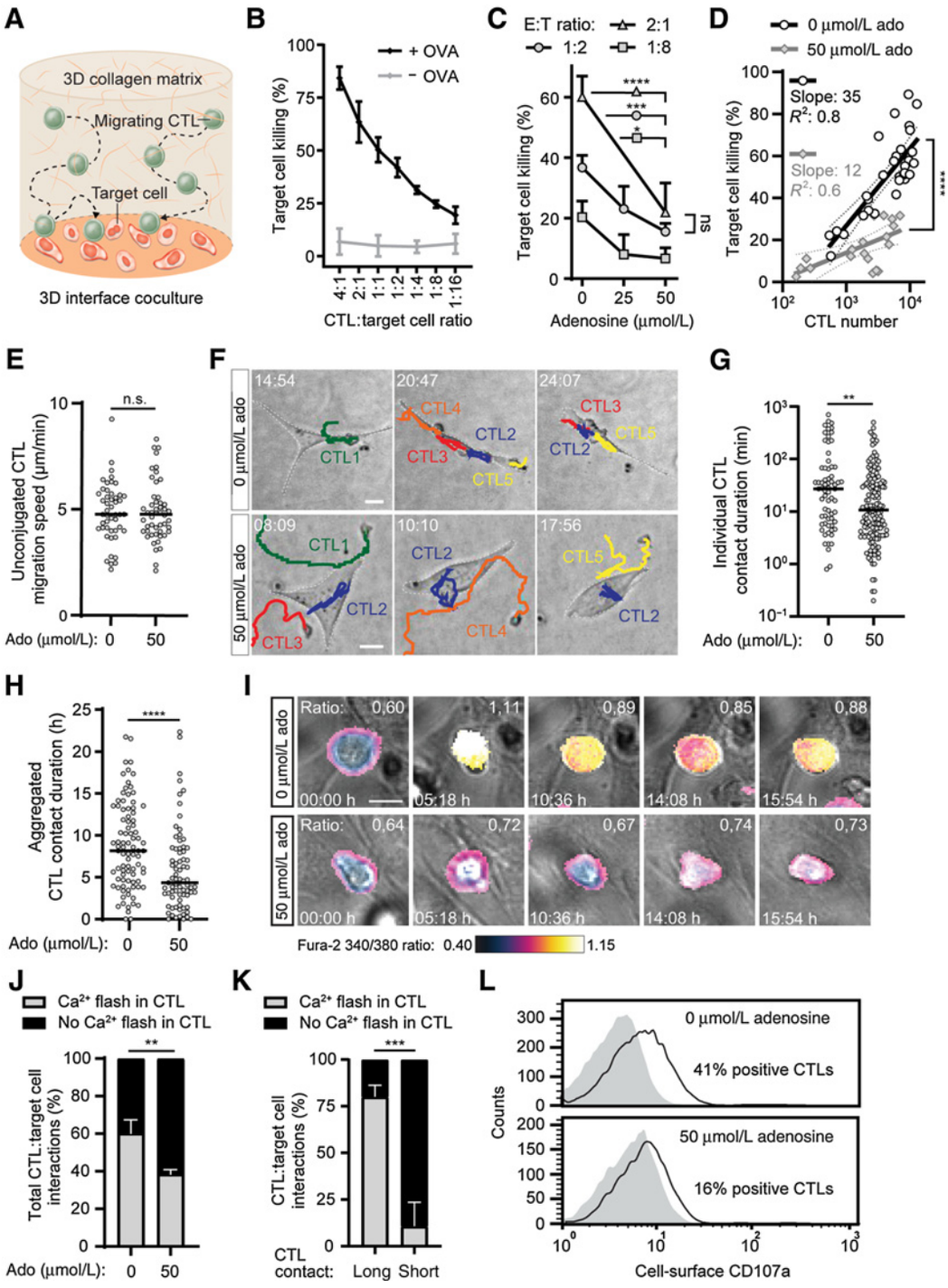

Figure 1.

Adenosine labilizes CTL–target cell interactions and compromises CTL killing efficacy. **A,** 3D interface coculture to monitor CTL-mediated killing of target cells. **B,** Killing of B16F10/OVA cells by OT-I CTLs at different E:T ratios after 30 hours of 3D interface coculture. Flow cytometry gating strategy in Supplementary Fig. S1a. Data represent the mean ± SD from 5 independent experiments, each performed in triplicate cultures. **C,** Killing of B16F10/OVA cells by OT-I T cells at different E:T ratios in the presence of various adenosine concentrations after 30 hours of 3D interface coculture. Data represent the mean ± SD from $N = 4$ independent experiments, each performed in triplicate cultures. Statistical differences, one-way ANOVA with Sidak *post hoc* test. **D,** Relationship between OT-I CTL numbers and B16F10/OVA cell killing after 30 hours of 3D interface coculture in the presence or absence of adenosine. Fitting by weighted nonlinear least squares regression (solid lines). Each regression curve was fitted based on $N = 54$ data points, with each data point representing a sample from 4 independent experiments. Dotted lines represent 95% confidence bands. Statistical differences, extra sum-of-squares F test comparing the slopes of the curves. (*Continued on the following page.*)

visualization. Quantification of OT-I CTL density, B16F10/OVA mitosis/apoptosis frequencies, and OT-I CTL mitosis/death rates was performed on individual image sections from 3D stacks. To preclude repeated counting of the same cell, every third slice per stack was analyzed. Nuclei and CTLs were segmented by Gaussian Blur filtering, automated thresholding (Bernsen's algorithm), and Watershed separation of touching objects. Objects were filtered for size (Nuclei: $\geq 80\,\mu m^2$) using the Analyze Particles command and counted per slice. To determine the B16F10/OVA apoptosis and mitosis frequencies from *in vivo* samples, apoptotic and mitotic nuclei were counted manually and calculated as the percentage of total nuclei per stack. Tumor subregions were defined manually, as follows: "edge" for cells located in the tumor mass within 300 µm from the tumor–stroma interface; and "center" for cells located >300 µm from the tumor margin. To quantify GCaMP6s intensity in B16F10/OVA tumors, background noise was reduced using a median filter (radius 2), followed by reconstruction of a maximum intensity Z-projection. The tumor boundary and ROI defining tumor subregions were manually segmented based on GCaMP6s expression in B16F10/OVA cells.

Statistical analysis

Parametric data sets were compared using an unpaired *t* test or one-way ANOVA. To correct for multiple comparisons, the one-way ANOVA was combined with Tukey or Sidak post-hoc testing. Nonparametric data sets were compared using the Mann–Whitney *U* or Kruskal–Wallis test. Dunn multiple comparisons correction was performed for Kruskal–Wallis testing. The extra sum-of-squares *F* test was used to compare the slopes of nonlinear regression curves on the relationship between OT-I CTL numbers and B16F10/OVA cell killing. Poisson regression was used to fit curves on the relationship between the CTL contact duration and the number of B16F10/OVA Ca^{2+} events per CTL contact. All data were analyzed using GraphPad Prism 9.

Data availability

The data generated in this study are available within the article and its supplementary data files.

Results

Adenosine labilizes CTL–target cell interactions and compromises killing efficacy

To identify the mechanisms by which extracellular adenosine compromised CTL effector functions against tumor cells, we used a 3D interface coculture of OT-I effector CTLs and B16F10/OVA melanoma cells (**Fig. 1A**). The 3D matrix environment of the 3D interface model depends on both active migration of CTLs to reach the lower tumor–matrix interface and recognition of the B16F10/OVA target cells (Supplementary Movie S1). Target cell killing increased with increasing CTL density, reaching up to 85% at a 4:1 CTL–target cell ratio (**Fig. 1B**; Supplementary Fig. S1a). The viability of B16F10 control cells, not expressing the OVA peptide, remained near 100%, irrespective of the E:T ratio (**Fig. 1B**). Low micromolar concentrations of adenosine, like those observed in tumors *in vivo* (34), reduced CTL-mediated tumor cell killing across a wide range of CTL densities and by up to 65% (**Fig. 1C**). A four-fold increase in CTL density, from E:T ratio of 1:2 to E:T ratio of 2:1, did not enhance B16F10/OVA cell killing under adenosine-rich conditions (**Fig. 1C**). The suppressive effect of adenosine on tumor cell killing by OT-I CTLs was caused by a dual effect: (i) lowering CTL numbers (by 45%) by reducing CTL proliferation without inducing direct CTL death (Supplementary Fig. S1b–S1d) and (ii) decreasing the killing rate per CTL, as indicated by a less steep slope of the regression curve between target cell killing and CTL density (**Fig. 1D**).

To investigate how adenosine affected CTL conjugation and target cell killing at the single-cell level, we performed time-lapse microscopy. Adenosine reduces T-cell crawling on ICAM-1–coated 2D substrates (22), and impaired CTL motility may delay the serial conjugation of CTLs with target cells. In 3D interface cocultures, adenosine did not affect the migration speed of OVA-stimulated OT-I CTLs during periods without target cell conjugation (**Fig. 1E**). However, adenosine shortened the CTL interaction time with individual tumor cells by 59%, from 27 minutes to 11 minutes (**Fig. 1F** and **G**; Supplementary Movie S1). The aggregated CTL contact duration with multiple tumor cells was reduced by 50%, from 8 to 4 hours (**Fig. 1H**). Thus, adenosine does not affect CTL migration speed in a 3D matrix environment but weakens CTL contact stability with target cells.

Next, we investigated the effect of adenosine on CTL calcium signaling and degranulation. During conjugation with B16F10/OVA cells, 60% of the OT-I CTLs underwent a phase of calcium signaling (**Fig. 1I** and **J**; Supplementary Movie S2). In the presence of adenosine, the CTL fraction exhibiting calcium flux was decreased by 20%. The reduction in CTL calcium signaling was associated with labile (<30 minutes) CTL–target cell interactions (**Fig. 1K**; Supplementary Movie S2). Consistent with decreased CTL reactivation, the surface expression of the CTL degranulation marker CD107a was also reduced under adenosine-rich conditions (**Fig. 1L**). Thus, adenosine labilizes CTL–target cell interactions, dampens calcium signaling and degranulation, and decreases CTL killing efficacy.

(*Continued.*) **E,** OT-I CTL migration speed in 3D interface cocultures in the absence (milliQ) or presence of adenosine during periods without conjugation to B16F10/OVA cells. Data points represent the average migration speed of individual CTLs during a tracking period of at least 1 hour. Horizontal lines, mean values from $N = 4$ independent experiments. Statistical differences, unpaired *t* test. **F,** Time-lapse sequence of OT-I CTLs engaging with B16F10/OVA cells in 3D interface cocultures in the absence (milliQ) or presence of adenosine. Colored lines represent 40-minute migration tracks of individual CTLs. Scale bar, 20 µm. Related to Supplementary Movie S1. **G** and **H,** Contact duration of OT-I CTLs with B16F10/OVA cells in the absence (milliQ) or presence of adenosine. Data points represent the contact duration of individual CTLs with (**G**) single or (**H**) multiple target cells during the final 20 hours of the 3D interface coculture. Horizontal lines, median values from $N = 67$–88 CTLs pooled from 4 independent experiments. Statistical differences, Mann–Whitney test. **I** and **J,** Ratiometric calcium imaging of fura-2–loaded OT-I T cells during the first hour of 3D interface coculture. **I,** Time-lapse sequence and (**J**) percentage of OT-I T cells with induced calcium flux during B16F10/OVA cell encounter in the absence (milliQ) or presence of adenosine. Data represent mean ± SD from $N = 4$ independent experiments. Statistical differences, unpaired *t* test. Time-lapse sequence related to Supplementary Movie S2. Scale bar, 10 µm. **K,** Percentage of fura-2–labeled OT-I T cells with induced calcium flux during B16F10/OVA cell encounter in 3D interface cocultures, stratified into long (≥30 minutes) and short (<30 minutes) CTL conjugates with the target cell monolayer. Data represent the mean ± SD from $N = 3$ independent experiments. Statistical differences, unpaired *t* test. **L,** Representative flow cytometry histograms of cell-surface CD107a expression by OT-I CTLs after 30 hours of coculture in the absence (milliQ) or presence of adenosine. Gray histogram, isotype control; solid line, CD107a. ns, not significant; *, $P \leq 0.05$; **, $P \leq 0.01$; ***, $P \leq 0.01$; ****, $P \leq 0.001$.

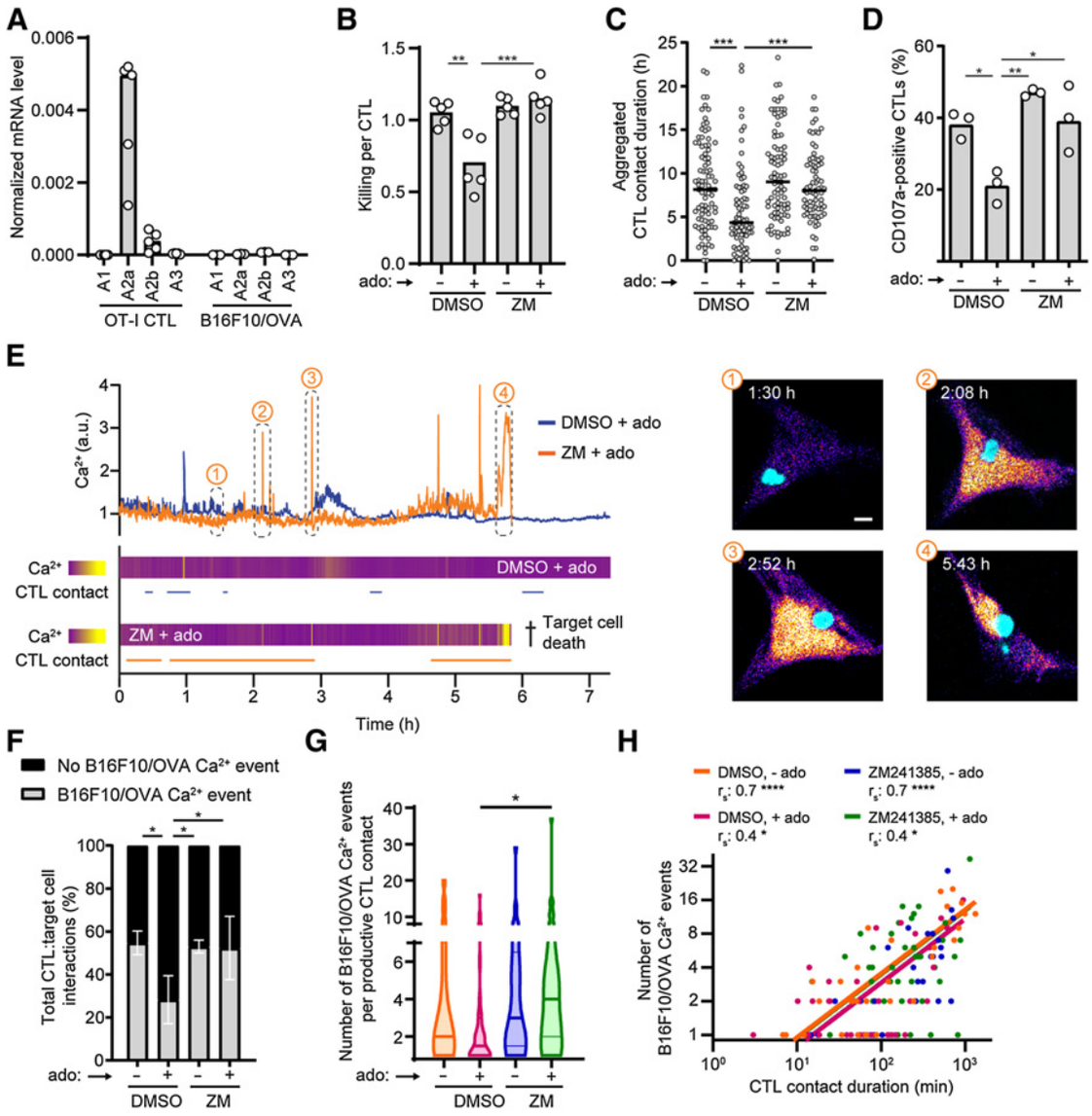

Figure 2.

Adenosine A2a receptor antagonism stabilizes CTL–target cell interactions, increases hit delivery, and restores single CTL efficacy in the presence of adenosine. **A,** mRNA expression of adenosine receptors in activated OT-I CTLs and IFNγ-stimulated B16F10/OVA cells. mRNA expression was normalized to the housekeeping genes Hprt1 and Gapdh. Each data point represents an independent experiment. Bars represent median values from 5 (OT-I CTLs) or 3 (B16F10/OVA cells) independent experiments. **B,** B16F10/OVA cell killing normalized to the number of CTLs after 30 hours of 3D interface coculture. Each data point represents an independent experiment. Bars represent mean values from $N = 5$ independent experiments, each performed in triplicate cultures. Statistical differences, one-way ANOVA with Tukey *post hoc* test. **C,** Contact duration of OT-I CTLs with B16F10/OVA cells. Data points represent the contact duration of individual CTLs with multiple target cells during the final 20 hours of 3D interface cocultures. Horizontal lines, median values from $N = 75$–84 CTLs pooled from 4 independent experiments. Statistical differences, Kruskal–Wallis test with Dunn *post hoc* correction. **D,** Cell-surface CD107a expression of OT-I CTLs after 30 hours of coculture. Each data point represents an independent experiment. Bars represent mean values from $N = 3$ independent experiments. Flow cytometry histograms in Supplementary Fig. S2b. Statistical differences, one-way ANOVA with Tukey *post hoc* test. **E,** Intensity plots and time-lapse sequence of the GCaMP6s sensor in B16F10/OVA cells showing a single CTL-associated B16F10/OVA Ca^{2+} event, followed by target cell survival in the presence of adenosine without ADORA2a antagonism (DMSO + ado) and multiple CTL-associated B16F10/OVA Ca^{2+} events followed by target cell death upon ADORA2a antagonism under adenosine-rich conditions (ZM + ado). Cyan, OT-I CTL. Fire LUT, GCaMP6s intensity. Scale bar, 10 μm. Related to Supplementary Movie S3. **F,** Percentage of CTL–tumor cell contacts that induced a Ca^{2+} event in B16F10/OVA cells. Data represent the mean ± SD from $N = 3$ (DMSO − ado, ZM241385 − ado, and ZM241385 + ado) or $N = 4$ (DMSO + ado) independent experiments. Statistical differences, one-way ANOVA with Tukey *post hoc* test. **G,** Number of Ca^{2+} events per individual CTL contact. Median (thick horizontal lines) and quartile values (thin horizontal lines) are based on $N = 29$–45 CTL–target cell interactions pooled from 3 to 4 independent experiments. **H,** Relationship between the CTL contact duration and the number of B16F10/OVA Ca^{2+} events per productive CTL contact. Each data point represents an individual CTL–target cell contact in 3D interface cocultures. The blue and green regression lines are not visible since they exactly overlap with the orange regression line. Fitting by Poisson regression from $N = 29$–45 CTL–target cell interactions pooled from $N = 3$–4 independent experiments. r_s, Spearman correlation coefficient. The 3D interface cocultures in all panels were treated with 50 μmol/L adenosine and 0.5 μmol/L ADORA2a antagonist ZM-241385 (ZM). *, $P \leq 0.05$; **, $P \leq 0.01$; ***, $P \leq 0.01$; ****, $P \leq 0.001$.

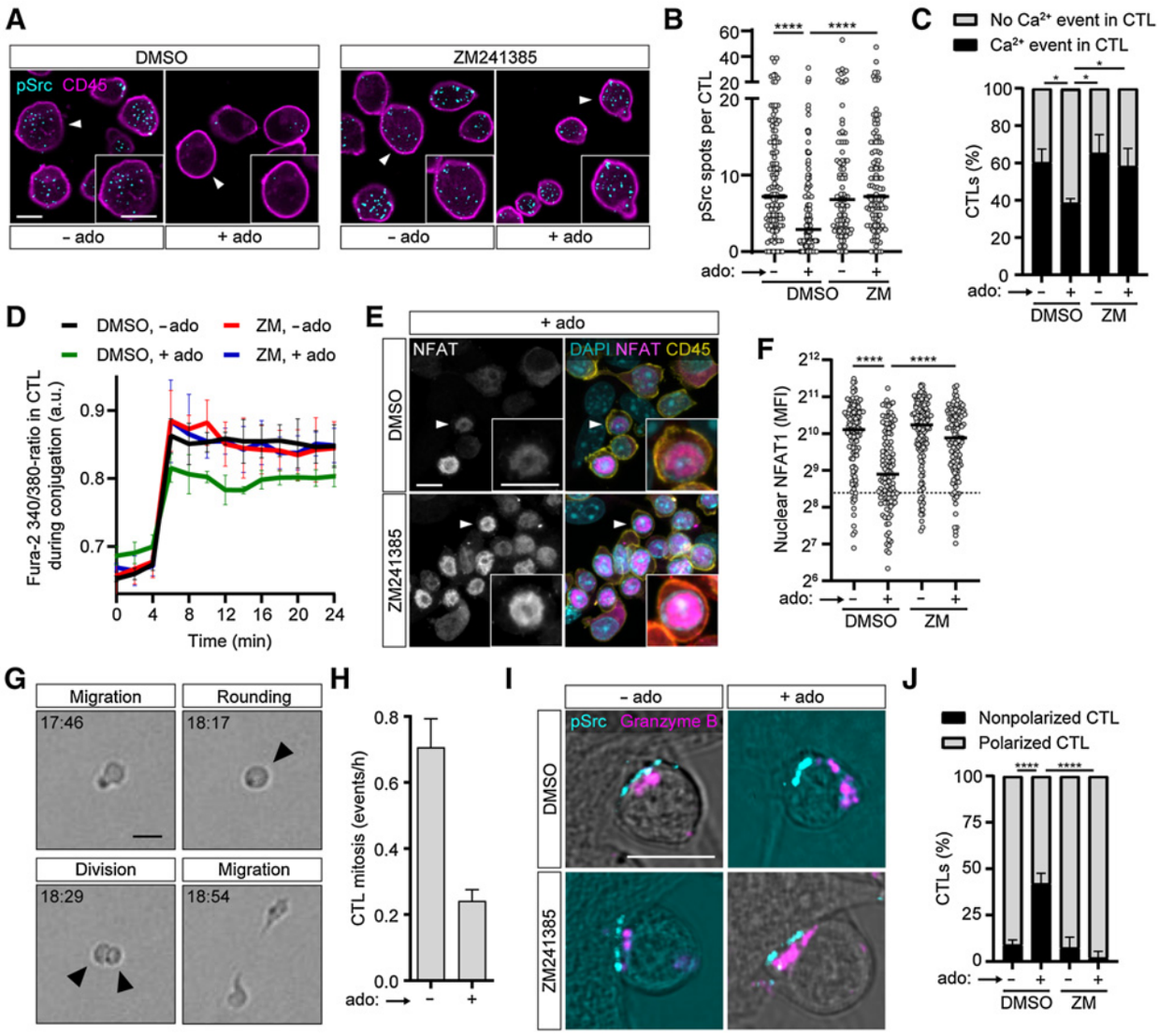

Figure 3.

ADORA2a triggering inhibits T-cell reactivation and impairs lytic granule polarization to the immune synapse of cytotoxic T cells. **A,** Representative micrographs and (**B**) quantification showing the number of phosphorylated (Tyr416) Src$^+$ microclusters in individual OT-I CTLs stimulated with immobilized anti-CD3 in the absence/presence of adenosine and ZM-241385 (ZM). Each data point represents the number of phospho-Src$^+$ microclusters within a single CTL. Arrowhead indicates a zoomed area (1.4-fold magnification of the overview image). Isotype control staining in Supplementary Fig. S3b and image quantification strategy in Supplementary Fig. S3c. Horizontal lines, median values from $N = 96–198$ CTLs pooled from 3 independent experiments. Statistical differences, Kruskal–Wallis test with a Dunn *post hoc* test. Scale bars, 10 μm. **C,** Percentage of Fura-2–loaded OT-I CTLs with induced calcium flux during B16F10/OVA cell encounter in the absence or presence of adenosine and ZM-241385 (ZM). Data represent the mean ± SD from $N = 4$ independent experiments. Statistical differences, one-way ANOVA with Tukey *post hoc* test. **D,** Calcium flux in Fura-2–loaded OT-I CTLs showing calcium mobilization during B16F10/OVA cell encounter in the absence or presence of adenosine and ZM-241385 (ZM). Data represent the mean ± SD from 4 independent experiments. **E,** Representative micrographs and (**F**) quantification of NFAT1 signal intensity in the nucleus of OT-I CTLs after 4 hours of coculture with B16F10/OVA cells in the absence or presence of adenosine and ZM-241385 (ZM). Arrowhead indicates a zoomed area (2.2-fold magnification of the overview image). Data represent the mean ± SD from $N = 3$ independent experiments. Statistical differences, Kruskal–Wallis test with Dunn *post hoc* correction. The dotted line represents the NFAT signal intensity in the nucleus of OT-I CTLs after 4 hours of coculture with B16F10 control cells (OVA peptide not expressed). **G,** Image sequence of CTL mitosis in 3D interface coculture of OT-I CTLs with B16F10/OVA cells. Arrowheads indicate cell division. Scale bar, 20 μm. Related to Supplementary Movie S4. **H,** Quantification of OT-I CTL mitosis rates in 3D interface cocultures of OT-I CTLs with B16F10/OVA cells in the presence or absence of adenosine. For each condition, CTL proliferation was analyzed in an area of 0.4 mm^2 obtained from a 30-hour time-lapse recording. Bars represent the mean ± SD from $N = 2$ independent experiments (0.71 and 0.24 CTL divisions per hour for 0 and 50 μmol/L adenosine, respectively). **I,** Representative micrographs and (**J**) percentage of conjugated CTLs with polarized granzyme B-containing cytotoxic granules after 4 hours of coculture in the absence/presence of adenosine and ZM-241385 (ZM). Only CTLs with a phosphorylated (Tyr416) Src$^+$ CTL-target cell contact were selected for analysis. Image quantification strategy in Supplementary Fig. S3e and definition of polarized/nonpolarized CTLs in Supplementary Fig. S3f. Data represent the mean ± SD from $N = 3$ independent experiments. Statistical differences, one-way ANOVA with Tukey *post hoc* test. All scale bars, 10 μm. The cultures in all figure panels were treated with 50 μmol/L adenosine and 0.5 μmol/L of the ADORA2a antagonist ZM-241385 (ZM). *, $P \leq 0.05$; **, $P \leq 0.01$; ***, $P \leq 0.01$; ****, $P \leq 0.001$.

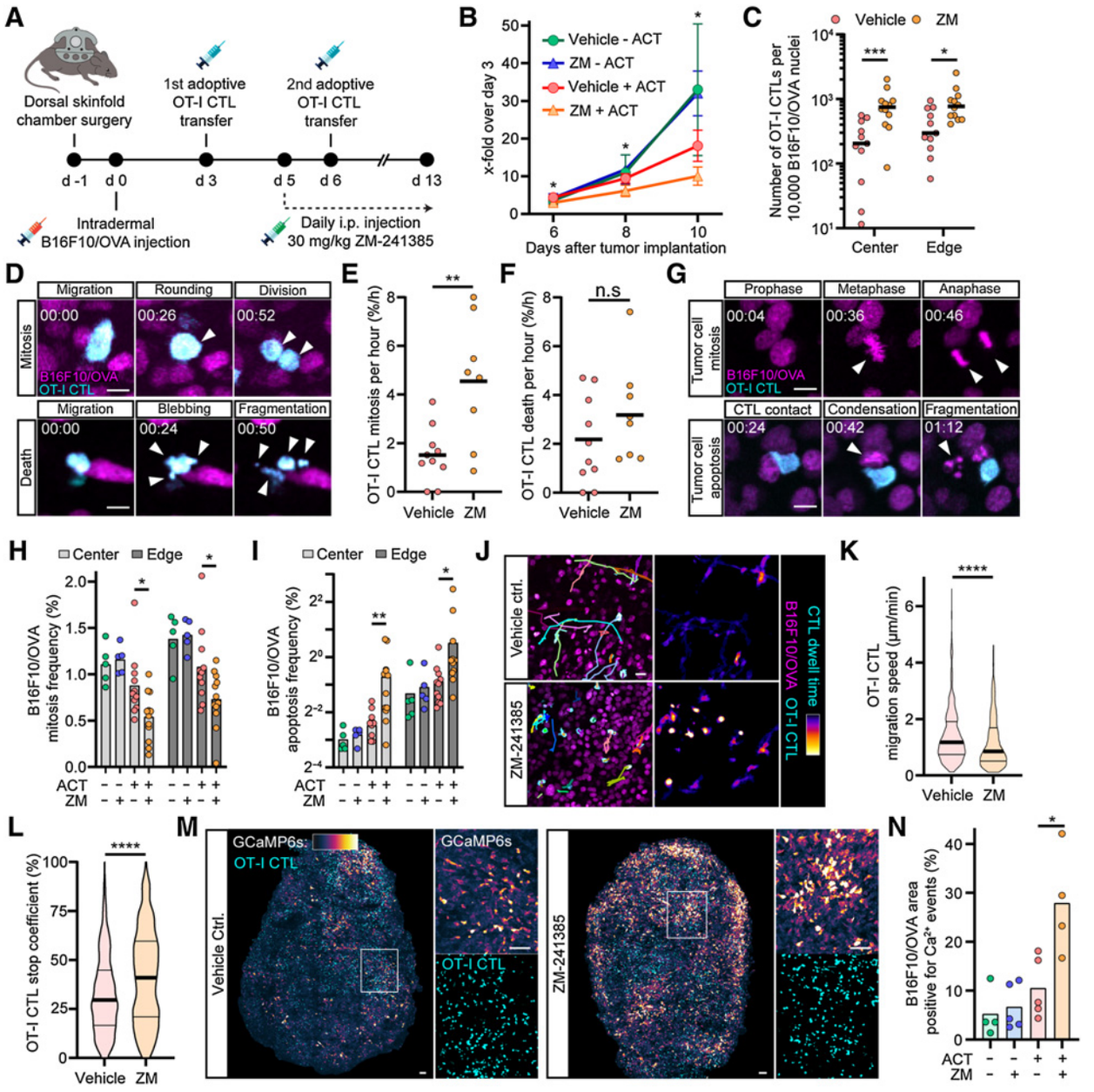

Figure 4.

ADORA2a antagonism supports CTL expansion, focused interaction, and cytotoxicity toward antigenic melanoma tumors *in vivo*. **A,** Experimental setup to monitor the effector response of adoptively transferred OT-I CTLs in progressing B16F10/OVA tumors upon treatment with vehicle or ZM-241385. **B,** B16F10/OVA tumor growth in mice treated with or without ACT and receiving vehicle or ZM-241385 (ZM). Data represent the mean volume ± SD from $N = 5$–6 independent tumors. Significance refers to the treatment conditions combined with OT-I CTL transfer (Supplementary Fig. S4), as calculated by a two-way ANOVA with Holm–Sidak *post hoc* test. **C,** Quantification of OT-I CTL density in the center and edge of B16F10/OVA tumors in mice treated with vehicle or ZM-241385 (ZM). Each data point represents an independent tumor monitored on day 6. Data were obtained from 3D stacks. Horizontal lines, mean values from $N = 11$–12 independent tumors. Statistical differences, two-way ANOVA with Sidak *post hoc* test. **D,** Image sequence of CTL mitosis and death in B16F10/OVA tumors. Arrowheads indicate cell division (mitotic CTL) or membrane blebbing and fragmentation (dying CTL). Scale bar, 10 µm. Related to Supplementary Movie S4. **E,** Quantification of OT-I CTL mitosis and (**F**) death rates in B16F10/OVA tumors in mice treated with vehicle or ZM-241385 (ZM) obtained from 60-minute 3D time-lapse recordings. Data points represent the means from at least 2 positions recorded per tumor ($N = 8$–10 independent tumors). Horizontal lines, mean values. Statistical differences, unpaired *t* test. **G,** Image sequence of B16F10/OVA mitosis and apoptosis visualized by histone-2B-mCherry. Arrowheads indicate metaphase and anaphase (mitotic cell) or condensation and fragmentation (apoptotic cell). Scale bar, 10 µm. **H** and **I,** Quantification of **(H)** B16F10/OVA mitosis and **(I)** apoptosis frequencies in mice treated with or without ACT and receiving vehicle or ZM-241385 (ZM). Data points represent the percentage of events from 3D stacks for each tumor, and bars represent the means from $N = 5$–12 independent tumors. Statistical differences, two-way ANOVA with Tukey *post hoc* test. **J,** OT-I CTL migration tracks (left) and dwell time (right) in B16F10/OVA tumors treated with vehicle or ZM-241385. Scale bar, 20 µm. Related to Supplementary Movie S5. (*Continued on the following page.*)

Adenosine-mediated inhibition of CTL effector responses is reversed by adenosine A2a receptor antagonism

We next explored how single CTL responses under adenosine-rich conditions could be restored. Adenosine mediates its biological effects by triggering adenosine transmembrane receptors (35). We profiled the expression of the known adenosine receptors in both OT-I and B16F10/OVA cells. Whereas B16F10/OVA cells did not express adenosine receptors above background levels, preactivated OT-I effector CTLs expressed the high-affinity ADORA2a abundantly, the low-affinity adenosine A2b receptor (ADORA2b) moderately, and none of the other adenosine receptors (**Fig. 2A**). Therefore, we hypothesized that adenosine compromised CTL effector functions via ADORA2a signaling. Indeed, under adenosine-rich conditions, the selective ADORA2a antagonist ZM-241385 completely restored the CTL killing efficacy to baseline levels (**Fig. 2B**). This immunostimulatory effect associated with prolonged CTL–tumor cell contacts and normalized CTL degranulation, which suggests that ADORA2a antagonism rescues the killing efficacy at the single CTL level (**Fig. 2C** and **D**; Supplementary Fig. S2a and S2b).

Adenosine A2a receptor antagonism restores CTL-mediated sublethal hit delivery in the presence of adenosine

CTL effector functions against melanoma target cells are inefficient with a high failure rate, and individual CTL–target cell contacts rarely induce apoptosis at first encounter (12). Solid tumor cells can thus survive individual sublethal cytotoxic hits. *In vivo*, effective target cell killing requires a cooperative process in which multiple CTLs engage sequentially with the same target cell to initiate apoptosis by a series of sublethal interactions (12). We tested whether microenvironmental perturbation by adenosine decreases the rate of sequential hits by CTLs and whether sequential hit delivery was restored upon ADORA2a antagonization. The calcium sensor GCaMP6s (27) expressed by B16F10/OVA was used to monitor transient Ca^{2+} influx through perforin pores during CTL engagement. The induction of Ca^{2+} influx, subsequent nuclear envelope rupture, and DNA damage are strictly dependent on perforin expression by OT-I CTLs, without effect of soluble cytokines (12). Identified by time-gated analysis, CTL-associated Ca^{2+} signals originated at the CTL-tumor cell contact region and can be reliably discriminated from unspecific intracellular Ca^{2+} fluctuations, based on their signal intensity and duration (12). In control cultures, CTLs induced a calcium event during 55% of the CTL–target cell contacts (**Fig. 2E** and **F**). The majority of these productive CTL contacts were highly efficient, as 69% induced 2 or more calcium events by the same CTL during a single contact (**Fig. 2G**; Supplementary Fig. S2c). The destabilizing effect of adenosine on CTL–tumor cell interactions associated with a 28% lower probability to induce a calcium event in target cells, with a 19% reduction in repetitive calcium induction by productive CTL contacts (**Fig. 2E–G**; Supplementary Fig. S2c; Supplementary Movie S3). Both contact duration and calcium induction in target cells were restored by ADORA2a antagonism under adenosine-rich conditions (**Fig. 2E–G**; Supplementary Fig. S2c; Supplementary Movie S3). The restored number of calcium events induced in the target cell was correlated with rescue in CTL contact duration (**Fig. 2H**). Thus, adenosine reduces contact efficacy by limiting contact duration, and this is reversed by ADORA2a antagonism, resulting in restored repetitive hit delivery and cytotoxicity.

Adenosine-induced ADORA2a triggering impairs the cytolytic immune synapse and lytic granule polarization

We next investigated the mechanism by which pharmacologic inhibition of adenosine-induced ADORA2a, triggering restored CTL contact efficacy. CTL conjugation is a multistep process that is orchestrated by TCR signaling in response to antigen recognition. Bulk population analysis by western blot has revealed that ADORA2a triggering suppresses anti-CD3–mediated TCR signaling in naïve CTLs (24). We validated these results for activated OT-I CTLs at the single-cell level by measuring activated Src kinases in individual CTLs stimulated with immobilized anti-CD3. Under control conditions, CD3 ligation by anti-CD3 induced phospho–Src-positive microclusters at the contact site/plane, with high cell-to-cell variability (**Fig. 3A** and **B**; Supplementary Fig. S3a–S3c). Adenosine reduced the number of phospho-Src^{+} microclusters by 60%, and this effect was completely restored by ADORA2a antagonism (**Fig. 3A** and **B**). We then performed ratiometric calcium imaging of fura-2–loaded OT-I CTLs cocultured with B16F10/OVA target cells to address whether a defective cytolytic synapse preceded target cell killing. Upon adenosine exposure, the fraction of CTLs with calcium mobilization decreased by 20% (**Fig. 3C**), and the amplitude of calcium influx into CTLs decreased under adenosine-rich conditions (**Fig. 3D**; Supplementary Fig. S3d), indicating weakened TCR signaling (36). Likewise, nuclear localization of the calcium-regulated nuclear factor of activated T cells 1 (NFAT1), a downstream effector of TCR activation and calcium signaling, was reduced (by 57%) upon OT-I CTL coculture with B16F10/OVA cells in the presence of adenosine (**Fig. 3E** and **F**). Thus, the strength of the CTL calcium influx, as well as downstream NFAT signaling, was dampened under adenosine-rich conditions. Both effects were completely rescued by ADORA2a antagonism with ZM-241385 (**Fig. 3C** and **F**).

The strength of CTL calcium signaling critically regulates CTL effector responses, mediating T-cell proliferation and cytotoxic granule exocytosis (37, 38). In OT-I CTLs, weakened calcium influx under adenosine-rich conditions associated with decreased proliferation (**Fig. 3G** and **H**; Supplementary Movie S4) and an increased frequency of conjugated CTLs that failed to polarize their cytotoxic granules toward the phospho-Src^{+} immune synapse (**Fig. 3I** and **J**; Supplementary Fig. S3e and S3f). Both effects were restored by ADORA2a antagonism (**Fig. 3I** and **J**; Supplementary Fig. S3g). Thus, triggering of the adenosine/ADORA2a pathway counteracts membrane-proximal TCR activation, calcium signaling, CTL proliferation, and lytic granule polarization to the immune synapse.

(*Continued.*) **K,** OT-I CTL migration speed during interaction with tumor cells and **(L)** stop coefficient in B16F10/OVA tumors treated with vehicle or ZM-241385 (ZM). The stop coefficient corresponds to relative amount of time that the CTL was arrested, as defined by a migration speed less than 0.5 μm/minute. CTLs were tracked for >20 minutes. Median (thick horizontal lines) and quartile values (thin horizontal lines) were based on $N = 453–538$ CTLs pooled from 5 independent tumors. **M,** GCaMP6s intensity and OT-I CTL density in B16F10/OVA tumors treated with vehicle or ZM-241385. The white box indicates the zoomed area (3.2-fold magnification of the overview image). Cyan, OT-I CTL. Morgenstemning LUT, GCaMP6s intensity. Scale bar, 100 μm. **N,** Relative B16F10/OVA tumor area positive for GCaMP6s Ca^{2+} events in mice treated with or without ACT and receiving vehicle or ZM-241385 (ZM). Each data point represents an independent tumor. Bars represent mean values from $N = 4–5$ independent tumors. Statistical differences, unpaired *t* test. Representative overview images of GCaMP6s intensity in B16F10/OVA tumors treated with vehicle or ZM-241385 without adoptive OT-I CTL transfer are shown in Supplementary Fig. S5. The data in **C–N** were acquired 6 days after tumor inoculation. ns, not significant; *, $P \leq 0.05$; **, $P \leq 0.01$; ***, $P \leq 0.01$; ****, $P \leq 0.001$.

ADORA2a antagonism supports CTL expansion and focuses CTL-mediated cytotoxicity in progressing melanoma tumors *in vivo*

To address the effect of ADORA2a antagonism on CTL effector function in progressing melanoma tumors *in vivo*, activated OT-I CTLs were adoptively transferred into C57BL/6J mice bearing intradermal B16F10/OVA tumors, and tumor growth was monitored by intravital microscopy through a skin window (**Fig. 4A**). Adoptive OT-I CTL transfer delayed the growth of B16F10/OVA tumors by 45%, and this effect was further enhanced (by 44%) when mice were treated with ZM-241385 (**Fig. 4B**; Supplementary Fig. S4a–S4c). The tumor growth–suppressing effect of ADORA2a antagonism was dependent on adoptive CTL transfer, as ZM-241385 treatment alone did not affect B16F10/OVA growth (**Fig. 4B**; Supplementary Fig. S4a and S4b). To directly address the effect of ADORA2a antagonism on CTL effector responses, we analyzed the expansion, effector dynamics, and function of tumor-infiltrating OT-I CTLs by long-term time-lapse microscopy. ADORA2a antagonism increased CTL density in tumors, both at the center (by 3.7-fold) and edge (by 2.6-fold; **Fig. 4C**), which resulted from enhanced CTL proliferation rates with unaffected CTL death (**Fig. 4D–F**; Supplementary Movie S5). The ADORA2a antagonist in combination with adoptive OT-1 CTL transfer affected tumor growth in both the tumor core and periphery, with reduced tumor cell mitosis rates and a 3.4-fold (center) and a 2.6-fold (edge) increase in tumor cell apoptosis rates (**Fig. 4G–I**). Besides increasing CTL density, ZM-241385 treatment reduced CTL migration speed (by 22%) and favored migration arrest of CTL subsets in contact with tumor cells (**Fig. 4J** and **L**; Supplementary Movie S5). When observed in conjunction, decreased migration speed and increased tumor cell death induction is indicative of more focused cognate antigen recognition and effector function (39). The *in vivo* interaction kinetics were consistent with the observed stabilization of CTL–target cell interactions by ADORA2a antagonism in adenosine-rich 3D interface cocultures (**Fig. 2C**). Visualization of GCaMP6s activity revealed that treatment with the ADORA2a antagonist induced a 3-fold increase in tumor areas positive for B16F10/OVA Ca^{2+} events (**Fig. 4M** and **N**). In contrast, in control tumors treated with vehicle or ZM-241385 without adoptive CTL transfer, the GCaMP6s^{+} tumor area remained unchanged (**Fig. 4M** and **N**; Supplementary Fig. S5a–S5b). Thus, ADORA2a antagonism does not induce damage in tumor cells directly, but its efficacy depends on the presence of adoptively transferred CTLs. In conclusion, combining adoptive CTL therapy with ADORA2a antagonism results in enhanced local CTL expansion and improved CTL effector function against tumor cells.

Discussion

The time-resolved single-cell analyses used in this study reveal that micromolar concentrations of adenosine, which match adenosine concentrations reached in tumors *in vivo* (34), interfere with multiple steps of the cytotoxic immune effector phase by (i) destabilizing CTL contacts with tumor cells, (ii) dampening proximal TCR signaling and downstream calcium influx, (iii) perturbing lytic granule polarization and exocytosis, and (iv) compromising sequential hit delivery and additive cytotoxicity. As a further consequence of impaired antigenic (re)stimulation, CTLs failed to expand in tumor lesions, resulting in reduced CTL numbers and cooperative engagements with tumor cells. This multilevel deterioration of CTL function was reverted by pharmacologic ADORA2a antagonization. ADORA2a inhibition restored tumor cell killing by stabilizing CTL–target cell conjugation and increasing sequential sublethal hit delivery to target cells, both *in vitro* and *in vivo*. Because enhanced adenosine signaling is a characteristic of a metabolically perturbed tumor microenvironment across solid tumor types, pharmacologic ADORA2a targeting may emerge as a critical supportive component for a range of immunotherapies.

Adenosine signaling perturbs multiple steps of CTL activation and antitumor effector function. Activation of the adenosine/ADORA2a pathway in naïve CTLs inhibits Src family tyrosine kinases (23), and inhibition of Src compromises CTL conjugation with DCs and subsequent T-cell activation (40). Similar to conjugation of naïve CTLs with DCs, we here showed that ADORA2a triggering by adenosine destabilizes conjugation of activated effector CTLs with target cells and severely limits sublethal hit delivery during individual contacts. Besides impairing lytic granule release, ADORA2a triggering has been shown to interfere with the production of CTL effector cytokines, including IFNγ and TNFα (21, 26, 41). Compromised cytokine secretion can be a consequence of instable CTL-target cell interaction and reduced CTL restimulation, for example, caused by experimental LFA-1 blockade, impaired TCR binding, or the presence of galectin-3 (42, 43). Thus, adenosine-induced labilization of CTL–target interaction and compromised antigenic restimulation may affect cell-mediated cytotoxicity and cytokine release in concert. The time-dependent integration of sublethal damaging events in cancer cells does not only depend on single CTL efficacy but also relies on a cooperative process in which multiple CTLs sequentially engage with the same target cell to induce apoptosis (12). Hence, by lowering the local density of CTLs, adenosine also compromises the serial delivery of perforin hits by CTL swarming. Delays in individual or cooperative hit delivery allow target cells to experience a prolonged time span between hits and, hence, an enhanced recovery time and chance to survive. Thus, ADORA2a signaling compromises both individual contact efficacy and CTL cooperativity required for serial killing of target cells.

The competitive antagonist ZM-241385 was used to inhibit ADORA2a signaling in effector CTLs. ZM-241385 exhibits high affinity for ADORA2a and dampens ADORA2a-mediated cAMP induction with an IC_{50} of 54 nmol/L (44), with 319-, 63-, and >10,000-fold selectivity over ADORA1, ADORA2b, and ADORA3, respectively (45). Therefore, at the concentration (0.5 μmol/L) used here in tumor-mimetic 3D cocultures, ZM-241385 was expected to selectively inhibit the adenosine/ADORA2a pathway in CTLs, while sparing ADORA2b signaling. ADORA2a antagonism in well-defined adenosine-rich cocultures enhanced CTL contact stability, improved lytic granule polarization and exocytosis, and increased the delivery of sublethal perforin hits per CTL contact. We also showed that ADORA2a antagonism restored the functionality of tumor-infiltrating CTLs in progressing melanoma lesions *in vivo* by inducing a local effector phenotype with prolonged dwell time and improved sublethal hit delivery. This rescue of CTL effector function likely underlies the ability of other small-molecule ADORA2a antagonists (25, 46, 47) and genetic ADORA2a targeting strategies (26, 48) to enhance the efficacy of ACT in solid tumors. Thus, ADORA2a antagonism reinvigorates the killing efficacy of tumor-infiltrating CTLs by normalizing their immune synapse function.

Besides increasing the CTL killing efficacy at the single-cell level, ADORA2a antagonism converted the moderately immune-infiltrated melanoma microenvironment, characterized by modest CTL density, into a more immune-inflamed microenvironment with dense CTL infiltrates. Consistent with enhanced antigenic restimulation, ADORA2a antagonism restored membrane-proximal TCR signaling, CTL calcium influx, and CTL proliferation in adenosine-

rich cocultures. ADORA2a antagonism also increased secondary expansion and swarming of tumor-infiltrating effector CTLs in B16F10/OVA tumors, thereby facilitating CTL cooperativity by serial CTL–tumor cell encounters (12). This increase in intratumoral CTL density has also been observed in renal cancer patients under active therapy with ADORA2a antagonists, which is associated with prolonged disease control in these patients (49). Similarly, expression of the ectonucleotidases CD39 and CD73 in preclinical tumor models suppresses the activation and proliferation of antigen-specific CTLs (46, 50). Thus, by supporting local CTL expansion in the tumor microenvironment, ADORA2a antagonism stimulates the cooperation of cytotoxic immune effector cells.

ZM-241385 has been used for proof-of-concept studies. Next-generation antagonists with extended *in vivo* half-life and good oral bioavailability have now been translated into the clinic, demonstrating tolerability and durable antitumor activity of adenosine antagonization regimens (49). Prolonged inhibition of ADORA2a is well tolerated in cancer patients, both as monotherapy and in combination with PD(L)-1 antibodies (49, 51, 52). To effectively target the adenosine/ADORA2a axis, predictive biomarkers are required to identify tumors that are under active adenosine-mediated immunosuppression and identify patients more likely to benefit from ADORA2a antagonists. As an example, gene-expression profiling can reveal ADORA2a signaling activity in the tumor microenvironment and identify patients with poor survival outcomes despite the accumulation of CTLs in tumor lesions (53). Besides its effect on CTL effector functions, adenosine signaling is known to inhibit NK cell maturation and impair perforin-mediated NK cell cytotoxicity against tumor cells (54, 55). Consequently, ADORA2a antagonism may exert a dual stimulatory effect on cumulative damage induction by reinvigorating effector responses of both tumor-infiltrating CTLs and NK cells (54). Thus, ADORA2a targeting may enable cooperation between cytotoxic leukocytes with complementary target-recognition strategies. The efficacy of ADORA2a targeting could be enhanced by combining ADORA2a antagonists with complementary approaches directed at increasing the susceptibility of tumor cells to sublethal damage, including radiotherapy to lower the setpoint of tumor cell apoptosis induction or DNA-repair inhibitors to delay target cell recovery between serial hits. Thus, ADORA2a antagonists can be positioned as an adjunct approach to other therapeutic strategies, with the aim to reinvigorate the CTL effector phase by normalizing immune synapse failure and CTL cooperativity in metabolically perturbed tumors.

Authors' Disclosures

None of the authors reported any disclosures.

Authors' Contributions

J. Slaats: Conceptualization, formal analysis, funding acquisition, validation, investigation, visualization, methodology, writing–original draft. **E. Wagena:** Formal analysis, validation, investigation, visualization, methodology. **D. Smits:** Formal analysis, investigation, visualization, methodology. **A.A. Berends:** Formal analysis, investigation, methodology. **E. Peters:** Software, formal analysis, investigation, methodology. **G.-J. Bakker:** Software, formal analysis, investigation, visualization, methodology. **M. van Erp:** Software, formal analysis, investigation, visualization, methodology. **B. Weigelin:** Conceptualization, formal analysis, supervision, validation, investigation, visualization, methodology. **G.J. Adema:** Conceptualization, formal analysis, supervision, validation, investigation, visualization, methodology, writing–original draft. **P. Friedl:** Conceptualization, formal analysis, supervision, funding acquisition, validation, investigation, visualization, methodology, writing–original draft.

Acknowledgments

This work was supported by a personal RadboudUMC PhD fellowship to J. Slaats (RvB15.52139). This work was also supported by grants from the European Research Council (617430-DEEPINSIGHT) and the Cancer Genomics Center to P. Friedl. Time-lapse confocal microscopy was enabled by an NWO investment grant to P. Friedl (834.13.003).

The publication costs of this article were defrayed in part by the payment of publication fees. Therefore, and solely to indicate this fact, this article is hereby marked "advertisement" in accordance with 18 USC section 1734.

Note

Supplementary data for this article are available at Cancer Immunology Research Online (http://cancerimmunolres.aacrjournals.org/).

Received February 13, 2022; revised July 30, 2022; accepted September 21, 2022; published first September 26, 2022.

References

1. Fridman WH, Zitvogel L, Sautes-Fridman C, Kroemer G. The immune contexture in cancer prognosis and treatment. Nat Rev Clin Oncol 2017; 14:717–34.
2. Peng W, Ye Y, Rabinovich BA, Liu C, Lou Y, Zhang M, et al. Transduction of tumor-specific T cells with CXCR2 chemokine receptor improves migration to tumor and antitumor immune responses. Clin Cancer Res 2010;16:5458–68.
3. Bulgarelli J, Tazzari M, Granato AM, Ridolfi L, Maiocchi S, de Rosa F, et al. Dendritic cell vaccination in metastatic melanoma turns "non-T cell inflamed" into "T-cell inflamed" tumors. Front Immunol. 2019;10:2353.
4. Andersen R, Donia M, Ellebaek E, Borch TH, Kongsted P, Iversen TZ, et al. Long-lasting complete responses in patients with metastatic melanoma after adoptive cell therapy with tumor-infiltrating lymphocytes and an attenuated IL2 regimen. Clin Cancer Res 2016;22:3734–45.
5. Goff SL, Dudley ME, Citrin DE, Somerville RP, Wunderlich JR, Danforth DN, et al. Randomized, prospective evaluation comparing intensity of lymphodepletion before adoptive transfer of tumor-infiltrating lymphocytes for patients with metastatic melanoma. J Clin Oncol 2016;34:2389–97.
6. Anguille S, Smits EL, Lion E, van Tendeloo VF, Berneman ZN. Clinical use of dendritic cells for cancer therapy. Lancet Oncol 2014;15:e257–67.
7. Lim AR, Rathmell WK, Rathmell JC. The tumor microenvironment as a metabolic barrier to effector T cells and immunotherapy. Elife 2020;9: e55185.
8. Fowell DJ, Kim M. The spatio-temporal control of effector T cell migration. Nat Rev Immunol 2021;21:582–96.
9. de la Roche M, Asano Y, Griffiths GM. Origins of the cytolytic synapse. Nat Rev Immunol 2016;16:421–32.
10. Friedl P, Weigelin B. Interstitial leukocyte migration and immune function. Nat Immunol 2008;9:960–9.
11. Masopust D, Schenkel JM. The integration of T cell migration, differentiation and function. Nat Rev Immunol 2013;13:309–20.
12. Weigelin B, den Boer AT, Wagena E, Broen K, Dolstra H, de Boer RJ, et al. Cytotoxic T cells are able to efficiently eliminate cancer cells by additive cytotoxicity. Nat Commun 2021;12:5217.
13. Blay J, White TD, Hoskin DW. The extracellular fluid of solid carcinomas contains immunosuppressive concentrations of adenosine. Cancer Res 1997;57: 2602–5.
14. Ohta A, Gorelik E, Prasad SJ, Ronchese F, Lukashev D, Wong MK, et al. A2A adenosine receptor protects tumors from antitumor T cells. Proc Natl Acad Sci U S A. 2006;103:13132–7.

15. Stagg J, Divisekera U, Duret H, Sparwasser T, Teng MW, Darcy PK, et al. CD73-deficient mice have increased antitumor immunity and are resistant to experimental metastasis. Cancer Res 2011;71:2892–900.
16. Loi S, Pommey S, Haibe-Kains B, Beavis PA, Darcy PK, Smyth MJ, et al. CD73 promotes anthracycline resistance and poor prognosis in triple negative breast cancer. Proc Natl Acad Sci U S A 2013;110:11091–6.
17. Allard B, Pommey S, Smyth MJ, Stagg J. Targeting CD73 enhances the antitumor activity of anti-PD-1 and anti-CTLA-4 mAbs. Clin Cancer Res 2013;19:5626–35.
18. Perrot I, Michaud HA, Giraudon-Paoli M, Augier S, Docquier A, Gros L, et al. Blocking antibodies targeting the CD39/CD73 immunosuppressive pathway unleash immune responses in combination cancer therapies. Cell Rep 2019;27: 2411–25.
19. Li XY, Moesta AK, Xiao C, Nakamura K, Casey M, Zhang H, et al. Targeting CD39 in cancer reveals an extracellular ATP- and inflammasome-driven tumor immunity. Cancer Discov 2019;9:1754–73.
20. Allard B, Allard D, Buisseret L, Stagg J. The adenosine pathway in immuno-oncology. Nat Rev Clin Oncol 2020;17:611–29.
21. Mastelic-Gavillet B, Navarro Rodrigo B, Decombaz L, Wang H, Ercolano G, Ahmed R, et al. Adenosine mediates functional and metabolic suppression of peripheral and tumor-infiltrating CD8(+) T cells. J Immunother Cancer 2019;7:257.
22. Chimote AA, Hajdu P, Kucher V, Boiko N, Kuras Z, Szilagyi O, et al. Selective inhibition of KCa3.1 channels mediates adenosine regulation of the motility of human T cells. J Immunol 2013;191:6273–80.
23. Vang T, Torgersen KM, Sundvold V, Saxena M, Levy FO, Skalhegg BS, et al. Activation of the COOH-terminal Src kinase (Csk) by cAMP-dependent protein kinase inhibits signaling through the T cell receptor. J Exp Med 2001;193: 497–507.
24. Linnemann C, Schildberg FA, Schurich A, Diehl L, Hegenbarth SI, Endl E, et al. Adenosine regulates CD8 T-cell priming by inhibition of membrane-proximal T-cell receptor signalling. Immunology 2009;128(1 Suppl):e728–37.
25. Kjaergaard J, Hatfield S, Jones G, Ohta A, Sitkovsky M. A2A adenosine receptor gene deletion or synthetic A2A antagonist liberate tumor-reactive CD8(+) T cells from tumor-induced immunosuppression. J Immunol 2018;201:782–91.
26. Giuffrida L, Sek K, Henderson MA, Lai J, Chen AXY, Meyran D, et al. CRISPR/Cas9 mediated deletion of the adenosine A2A receptor enhances CAR T cell efficacy. Nat Commun 2021;12:3236.
27. Chen TW, Wardill TJ, Sun Y, Pulver SR, Renninger SL, Baohan A, et al. Ultrasensitive fluorescent proteins for imaging neuronal activity. Nature 2013;499:295–300.
28. Bohm W, Thoma S, Leithauser F, Moller P, Schirmbeck R, Reimann J. T cell-mediated, IFN-gamma-facilitated rejection of murine B16 melanomas. J Immunol 1998;161:897–908.
29. Weigelin B, Bolanos E, Teijeira A, Martinez-Forero I, Labiano S, Azpilikueta A, et al. Focusing and sustaining the antitumor CTL effector killer response by agonist anti-CD137 mAb. Proc Natl Acad Sci U S A 2015;112:7551–6.
30. Haeger A, Alexander S, Vullings M, Kaiser FMP, Veelken C, Flucke U, et al. Collective cancer invasion forms an integrin-dependent radioresistant niche. J Exp Med 2020;217:e20181184.
31. Preibisch S, Saalfeld S, Tomancak P. Globally optimal stitching of tiled 3D microscopic image acquisitions. Bioinformatics 2009;25:1463–5.
32. Thevenaz P, Ruttimann UE, Unser M. A pyramid approach to subpixel registration based on intensity. IEEE Trans Image Process 1998;7:27–41.
33. Parslow A, Cardona A, Bryson-Richardson RJ. Sample drift correction following 4D confocal time-lapse imaging. J Vis Exp 2014:51086.
34. Vaupel P, Mayer A. Hypoxia-driven adenosine accumulation: a crucial microenvironmental factor promoting tumor progression. Adv Exp Med Biol 2016; 876:177–83.
35. Vijayan D, Young A, Teng MWL, Smyth MJ. Targeting immunosuppressive adenosine in cancer. Nat Rev Cancer 2017;17:709–24.
36. Beal AM, Anikeeva N, Varma R, Cameron TO, Vasiliver-Shamis G, Norris PJ, et al. Kinetics of early T cell receptor signaling regulate the pathway of lytic granule delivery to the secretory domain. Immunity 2009;31:632–42.
37. Kim KD, Bae S, Capece T, Nedelkovska H, de Rubio RG, Smrcka AV, et al. Targeted calcium influx boosts cytotoxic T lymphocyte function in the tumour microenvironment. Nat Commun 2017;8:15365.
38. Slaats J, Dieteren CE, Wagena E, Wolf L, Raaijmakers TK, van der Laak JA, et al. Metabolic screening of cytotoxic T-cell effector function reveals the role of CRAC channels in regulating lethal hit delivery. Cancer Immunol Res 2021;9:926–38.
39. Boissonnas A, Fetler L, Zeelenberg IS, Hugues S, Amigorena S. In vivo imaging of cytotoxic T cell infiltration and elimination of a solid tumor. J Exp Med 2007;204: 345–56.
40. Wiemer AJ, Hegde S, Gumperz JE, Huttenlocher A. A live imaging cell motility screen identifies prostaglandin E2 as a T cell stop signal antagonist. J Immunol 2011;187:3663–70.
41. Sorrentino C, Hossain F, Rodriguez PC, Sierra RA, Pannuti A, Osborne BA, et al. Adenosine A2A receptor stimulation inhibits TCR-induced Notch1 activation in $CD8^+$ T cells. Front Immunol 2019;10:162.
42. Sanderson NS, Puntel M, Kroeger KM, Bondale NS, Swerdlow M, Iranmanesh N, et al. Cytotoxic immunological synapses do not restrict the action of interferon-gamma to antigenic target cells. Proc Natl Acad Sci U S A 2012;109:7835–40.
43. Petit AE, Demotte N, Scheid B, Wildmann C, Bigirimana R, Gordon-Alonso M, et al. A major secretory defect of tumour-infiltrating T lymphocytes due to galectin impairing LFA-1-mediated synapse completion. Nat Commun 2016;7: 12242.
44. Uustare A, Vonk A, Terasmaa A, Fuxe K, Rinken A. Kinetic and functional properties of [3H]ZM241385, a high affinity antagonist for adenosine A2A receptors. Life Sci 2005;76:1513–26.
45. Ongini E, Dionisotti S, Gessi S, Irenius E, Fredholm BB. Comparison of CGS 15943, ZM 241385 and SCH 58261 as antagonists at human adenosine receptors. Naunyn Schmiedebergs Arch Pharmacol 1999;359:7–10.
46. Jin D, Fan J, Wang L, Thompson LF, Liu A, Daniel BJ, et al. CD73 on tumor cells impairs antitumor T-cell responses: a novel mechanism of tumor-induced immune suppression. Cancer Res 2010;70:2245–55.
47. Leone RD, Sun IM, Oh MH, Sun IH, Wen J, Englert J, et al. Inhibition of the adenosine A2a receptor modulates expression of T cell coinhibitory receptors and improves effector function for enhanced checkpoint blockade and ACT in murine cancer models. Cancer Immunol Immunother 2018;67:1271–84.
48. Beavis PA, Henderson MA, Giuffrida L, Mills JK, Sek K, Cross RS, et al. Targeting the adenosine 2A receptor enhances chimeric antigen receptor T cell efficacy. J Clin Invest 2017;127:929–41.
49. Fong L, Hotson A, Powderly JD, Sznol M, Heist RS, Choueiri TK, et al. Adenosine 2A receptor blockade as an immunotherapy for treatment-refractory renal cell cancer. Cancer Discov 2020;10:40–53.
50. Kashyap AS, Thelemann T, Klar R, Kallert SM, Festag J, Buchi M, et al. Antisense oligonucleotide targeting CD39 improves anti-tumor T cell immunity. J Immunother Cancer 2019;7:67.
51. Powderly JD, S PLd, Gutierrez R, Horvath L, Seitz L, Ashok D, et al. AB928, a novel dual adenosine receptor antagonist, combined with chemotherapy or AB122 (anti-PD-1) in patients (pts) with advanced tumors: preliminary results from ongoing phase I studies. J Clin Oncol 2019;37(15 suppl):2604.
52. Chiappori A, Williams CC, Creelan BC, Tanvetyanon T, Gray JE, Haura EB, et al. Phase I/II study of the A2AR antagonist NIR178 (PBF-509), an oral immunotherapy, in patients (pts) with advanced NSCLC. J Clin Oncol 2018;36 (15_suppl):9089.
53. Sidders B, Zhang P, Goodwin K, O'Connor G, Russell DL, Borodovsky A, et al. Adenosine signaling is prognostic for cancer outcome and has predictive utility for immunotherapeutic response. Clin Cancer Res 2020;26:2176–87.
54. Raskovalova T, Huang X, Sitkovsky M, Zacharia LC, Jackson EK, Gorelik E. Gs protein-coupled adenosine receptor signaling and lytic function of activated NK cells. J Immunol 2005;175:4383–91.
55. Young A, Ngiow SF, Gao Y, Patch AM, Barkauskas DS, Messaoudene M, et al. A2AR adenosine signaling suppresses natural killer cell maturation in the tumor microenvironment. Cancer Res 2018;78:1003–16.